OL | Organic Letters

Letter

Cite This: Org. Lett. XXXX, XXX, XXX−XXX

pubs.acs.org/OrgLett

# Photocontrolled Single-/Dual-Site Alternative Fluorescence Probes Distinguishing Detection of $H_2S/SO_2$ in Vivo

Weijie Zhang,[†] Fangjun Huo,[‡] and Caixia Yin*[,†]

[†]Key Laboratory of Chemical Biology and Molecular Engineering of Ministry of Education, Key Laboratory of Materials for Energy Conversion and Storage of Shanxi Province, Institute of Molecular Science, Shanxi University, Taiyuan 030006, China

[‡]Research Institute of Applied Chemistry, Shanxi University, Taiyuan 030006, China

Supporting Information

**ABSTRACT:** Herein, a novel fluorescent probe by integrating 4-azide-1,8-naphthalic anhydride and spiropyran was obtained. **NT-$N_3$-SP** was capable of specifically monitoring $H_2S$ by azide reduced. Upon irradiation by alternate ultraviolet and visible light, both the structure and emission of spiropyran moiety in **NT-$N_3$-SP** can be reversibly tuned. Importantly, the alternation will be interrupted in the presence of $SO_2$. Additionally, **NT-$N_3$-SP** was successfully used for detection of $H_2S/SO_2$ in cells and mice.

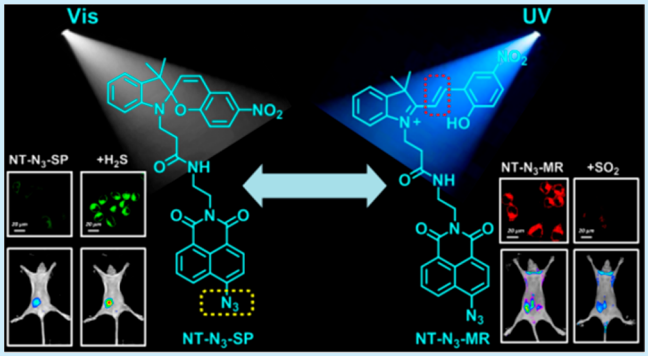




Reactive sulfur species (RSS) are a class of sulfur-containing compounds that play vital roles in human physiology.[1−3] Among these RSS, hydrogen sulfide ($H_2S$) and sulfur dioxide ($SO_2$) seem to be the most attractive sulfur compounds due to their physiological role as the endogenous gasotransmitters following nitric oxide (NO) and carbonic oxide (CO).[4−9] From a chemistry perspective, $H_2S$ and $SO_2$ are redox partners; therefore, they could coexist in biological systems. In fact, it is evident that $SO_2$ and $H_2S$ are generated from the same metabolism of sulfur-containing amino acids, and sometimes the two gasotransmitters share the same signal pathway, even the same target residue.[10−13] In addition, increasing studies suggested that $H_2S$ and $SO_2$ exhibit similar anti-inflammatory activities against ROS, especially in cardiovascular systems.[14] Obviously, there is a significant correlation between $H_2S$ and $SO_2$ in the living systems. Because of these similar properties, researchers cannot distinguish one specific from another in the complicated physiological environment of the cells. In fact, some biological mechanisms that were originally attributed to $H_2S$ may actually be mediated by $SO_2$ and vice versa.

In order to better understand the physiological roles of $SO_2$ and $H_2S$, several methods, such as electrochemistry, chromatography, and capillary electrophoresis, have been reported for $SO_2$[15−18] and $H_2S$[19,20] detection. However, these methods cannot be directly applied to living cells due to their destructive nature.[21] Fluorescence probes, which can display rapid, noninvasive, and sensitive detection of target analytes, have become powerful tools for in vivo imaging.[22−25] Although a few fluorescent probes for the detection of $SO_2$ or $H_2S$ have been reported in recent years, most still suffer from drawbacks in terms of the selectivity. The design of a single fluorescent probe which displays a highly selective and distinctive response for $H_2S$ and $SO_2$ simultaneously is highly desirable but even more challenging. Studies suggest that the aryl azide group shows high selectivity with hydrogen sulfide.[26,27] Therefore, we speculate that azide derivative seems to be an ideal probe for $H_2S$ detection. Spiropyran, as a typical photoswitchable molecule,[28−30] was a latent fluorophore that can be reversibly tuned to merocyanine, which shows high selectivity for $SO_2$ detection.[31] To this end, we coupled the spiropyran derivative to the weakly fluorescent molecule 4-azide-1,8-naphthalic anhydride with ethylenediamine as a tether. The full working strategy is described in Scheme 1.

In order to confirm our hypothesis for $SO_2$ and $H_2S$ detection, first we tested the absorbance and fluorescence responses of **NT-$N_3$-SP** with UV irradiation. As expected, upon irradiation of UV light (365 nm, 12W), a gradual fluorescence emission at 630 nm

**Scheme 1. Molecular Structure and Proposed Sensing Mechanism of NT-$N_3$-SP for $H_2S$ and $SO_2$**

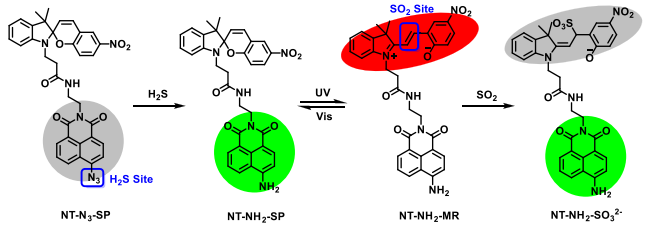


**Received:** May 31, 2019




DOI: 10.1021/acs.orglett.9b01879
Org. Lett. XXXX, XXX, XXX−XXX

was observed (Figure 1a), which fully proved the formation of MR isomer. In addition, with the photoconversion of the SP

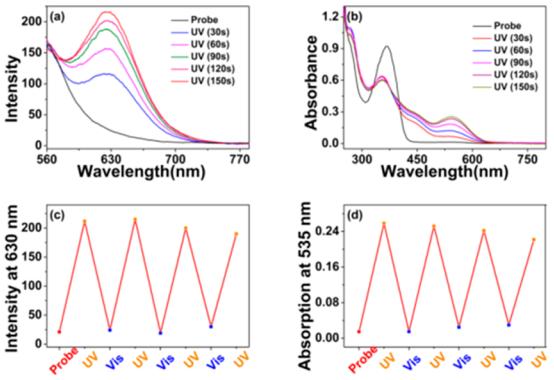


**Figure 1.** (a) Fluorescence spectra and (b) absorption spectra of probe **NT-$N_3$-SP** (10 $\mu$M) upon irradiation with a UV lamp. (c) Fluorescence emission and (d) UV−vis absorbance photoswitching of **NT-$N_3$-SP** with UV/vis cycle. Test medium: PBS/$C_2H_5OH$ solution (v/v = 1/1, pH 7.4).

moiety, the azide group was also reduced, and the absorption peaks at 440 and 535 nm are enhanced during the UV irradiation (Figure 1b). The light-controlled reversible SP/MR switch could be realized for several cycles without obvious degradation in intensity (Figure 1c,d).

Then UV−vis and fluorescence measurements were carried out. As described in Figure 2a, upon addition of $Na_2S$ (0−200

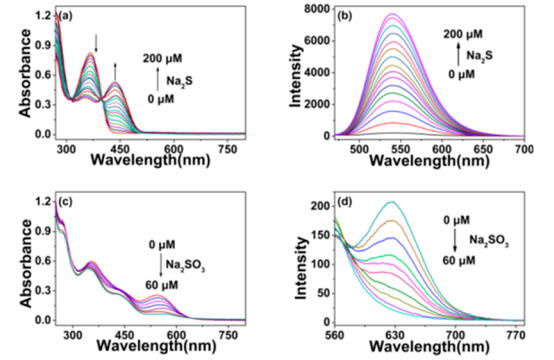


**Figure 2.** (a) Absorption spectra and fluorescence spectra changes of probe **NT-$N_3$-SP** (10 $\mu$M) with increasing $Na_2S$ (0−200 $\mu$M), $\lambda_{ex}$ = 440 nm. (c) Fluorescence emission and (d) UV−vis absorbance of activated **NT-$NH_2$-MR** (10 $\mu$M) in the presence of $Na_2SO_3$ (60 $\mu$M), $\lambda_{ex}$ = 535 nm.

$\mu$M), the maximal absorption at 370 nm decreased and a new red-shifted absorbance peak at 440 nm was centered. Meanwhile, the fluorescence intensity was significantly enhanced at 540 nm (Figure 2b), and the detection limit of **NT-$N_3$-SP** for $Na_2S$ was calculated to be 0.101 $\mu$M (Figure S1a) based on IUPAC (CDL = $3S_b/m$).[32,33]

Probe **NT-$N_3$-SP** is essentially nonfluorescent at around 630 nm due to the ring-closed spiropyran moiety. In addition, the presence of $Na_2SO_3$ caused almost no changes in the absorption and fluorescence spectra, suggesting that the caged compound is stable and it will not transform into the fluorescence form without UV irradiation. In contrast, upon 150 s UV irradiation, a huge enhancement of **NT-$NH_2$-MR** in both the absorption and fluorescence spectra was observed as shown in Figure S2a,b. Then the UV light-controlled recognition of **NT-$NH_2$-SP** for $SO_2$ was performed in solution. The decrease of the maximum absorption band around 535 nm confirmed the disruption of the double bond in the merocyanine moiety (Figure 2c). Simultaneously, the fluorescent emission at 630 nm decreased gradually with the addition of $Na_2SO_3$ (Figure 2d), suggesting formation of the Michael adduct between $Na_2SO_3$e and MR-stat. The detection limit of **NT-$NH_2$-MR** toward the $SO_2$ derivative was calculated to be 0.121 $\mu$M (Figure S3).

We then tested the selectivity of **NT-$N_3$-SP** for $H_2S$ and $SO_2$. It was found that only the addition of $Na_2S$ induced significant fluorescence enhancement at 540 nm (Figure S4a). Next, we recorded the spectra change of **NT-$N_3$-MR** with other analytes. As shown in Figure S4b, other interfering species hardly caused any fluorescence change at 630 nm except $Na_2SO_3$. Then the real-time fluorescence responses of **NT-$N_3$-SP** toward $SO_2$ and $H_2S$ were examined by recording the fluorescence intensity of the two emission wavelengths at 540 or 630 nm, respectively. As illustrated in Figure S5a, the fluorescence intensity at 540 nm notably enhanced and finally leveled off at around 25 min after treatment with 200 $\mu$M $Na_2S$. The fluorescence signals of **NT-$NH_2$-MR** at 630 nm leveled off within 5 min upon addition of $Na_2SO_3$ (200 $\mu$M), suggesting that the MR state is highly reactive with $SO_2$. However, one may wonder if hydrogen sulfide may also show high reactivity toward such a conjugated system. To address this issue, we further investigated the time-dependent fluorescence response of **NT-$NH_2$-MR** at 630 nm with hydrogen sulfide. Upon addition of $Na_2S$, the fluorescence signals at 630 nm decreased more slowly than those of $SO_2$, and the detection process was still ongoing until 60 min (Figure S5c). As a result, the azido group seems to be more sensitive toward $H_2S$ compared with the MR state in **NT-$NH_2$-MR**. The pH effect of **NT-$N_3$-SP** toward $SO_2$ and $H_2S$ was subsequently investigated. Probe **NT-$N_3$-SP** is stable in a broad pH range (3.0−8.0), and an obvious enhancement of intensity at 540 nm was found after it was treated with $Na_2S$ within the normal physiological ranges from 5.0 to 7.4 (Figure S6a). **NT-$NH_2$-MR** was also steady in a broad pH range (3.0−8.0) after UV irradiation, and the addition of $Na_2SO_3$ displayed the best fluorescence response within the pH range from 5.0 to 8.0 (Figure S6b).

For the mechanistic study of probe **NT-$N_3$-SP** for $H_2S$ and $SO_2$, the mass spectrometry analysis was carried out here. ESI-MS in Figure S7a shows a main peak at $m/z$ 644.22525 $[M - H]^+$, which corresponds to **NT-$N_3$-SP**. The mass peak appearing at $m/z$ 618.23474 corresponded to the product of **NT-$N_3$-SP** with $Na_2S$ (Figure S7b). Then the mixture of **NT-$N_3$-SP** with $Na_2S$ was exposed to UV light. As expected, MS analysis gave the expected mass shift at $m/z$ 618.23444 of deserved product **NT-$NH_2$-MR**, and the dominant peaks at 640.21674 were attributed to the complex of **NT-$NH_2$-MR** + Na (Figure S7c). Additionally, it is worth pointing out no signal appeared at 651.2152 in the mass spectrometry, which should belong to **NT-$NH_2$-MR** + $Na_2S$ (Figure S7d). However, a noticeable signal peak was observed at $m/z$ 698.1931 with the mixture of **NT-$NH_2$-SP** + $Na_2SO_3$ (Figure S7e). All these results were consistent with our hypothesis.

Next, fluorescence imaging in living cells was carried out. First, the cytotoxicity of **NT-$N_3$-SP** was evaluated by MTT assay (Figure S8), and the result showed that **NT-$N_3$-SP** was well suited for bioimaging applications. We then carried out fluorescence imaging of exogenous $H_2S$ and endogenous $H_2S$ (induced by SNP: sodium nitroprusside). As shown in Figure 3


DOI: 10.1021/acs.orglett.9b01879
Org. Lett. XXXX, XXX, XXX−XXX

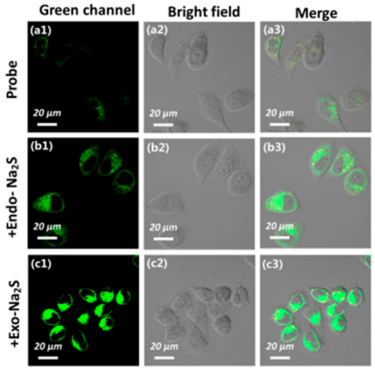


**Figure 3.** Confocal microscopy images of living HepG 2 cells. (a1−a3) Fluorescence imaging probe **NT-$N_3$-SP** (10 $\mu$M). (b1−b3) Fluorescence imaging probe **NT-$N_3$-SP** (10 $\mu$M) with endogenous $H_2S$ (induced by SNP). (c1−c3) Fluorescence imaging probe **NT-$N_3$-SP** (10 $\mu$M) with exogenous $H_2S$ ($Na_2S$: 50 $\mu$M). Green channel $\lambda_{em}$ = 530 ± 20 nm ($\lambda_{ex}$ = 458 nm).

(b1), after pretreatment with SNP (500 $\mu$M) for 60 min, the cells incubated with **NT-$N_3$-SP** showed an enhancement in fluorescence in green channel. Similarly, a remarkable enhancement of the green fluorescence signal was observed when **NT-$N_3$-SP** pretreated cells were further incubated with $Na_2S$ for 20 min, which indicates that **NT-$N_3$-SP** was capable of monitoring both exogenous and endogenous $H_2S$ in living cells.

Then **NT-$N_3$-SP**-loaded HepG 2 cells were treated with UV light for conversion to the **MR** state. It is also known that UV causes photobleaching of azide-containing dyes. As a result of the Förster resonance energy transfer (FRET) from naphthalimide donor to the MR acceptor, it was found that HepG 2 cells showed negligible fluorescence in the green channel but a strong fluorescence in the red channel after 3 min of UV irradiation (Figure 4b). To our delight, after the visible-light

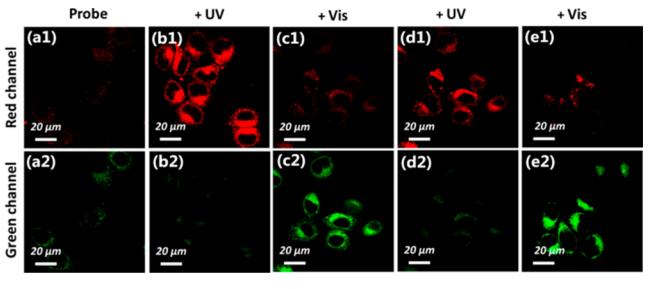


**Figure 4.** Photochromism of probe **NT-$N_3$-SP** in living cells. (a1, a2) HepG 2 cells were first incubated with probe **NT-$N_3$-SP** (10 $\mu$M). (b1, b2): Cells were further treated with $Na_2S$ (100 $\mu$M). (c1−f1, c2−f2): UV/vis cycling of the two imaging channels of **NT-$NH_2$-MR** and **NT-$NH_2$-SP**. Red channel $\lambda_{em}$ = 630 ± 20 nm ($\lambda_{ex}$ = 561 nm), green channel $\lambda_{em}$ = 535 ± 20 nm ($\lambda_{ex}$ = 458 nm).

irradiation (10 min), the fluorescence was recovered due to the reversible isomerization from the MR state back to the initial SP state (Figure 4c). Furthermore, we obtained satisfactory intracellular photochromic actions with alternate UV/vis irradiation (Figure 4d,e). As a whole, these results clearly validate the smart light-control of **NT-$N_3$-SP** by alternate UV/vis irradiation in living cells.

Eventually, the UV light-controlled conversion of **NT-$N_3$-SP** from the SP state to the activated MR state for $SO_2$ detection was carried out in HepG 2 cells. Probe **NT-$N_3$-SP** was first internalized by HepG 2 cells and then treatment with UV light irradiation for 3 min (a1). Subsequently, we tested the ability of **NT-$NH_2$-MR** for imaging endogenous $SO_2$ induced by lipopolysaccharide (LPS: 1 $\mu$g/mL). As shown in Figure 5 (b1),

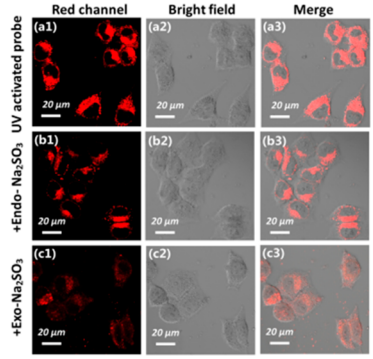


**Figure 5.** Confocal microscopy images of $Na_2SO_3$ in living HepG2 cells. (a1−a3) Cells were pretreated with probe **NT-$N_3$-SP** (10 $\mu$M) and then treated with UV irradiation. (b1−b3) Fluorescence imaging of UV-activated probe **NT-$N_3$-SP** (10 $\mu$M) with endogenous $SO_2$ (induced by LPS). (c1−c3) Fluorescence imaging of UV-activated probe **NT-$N_3$-SP** (10 $\mu$M) with exogenous $SO_2$ ($Na_2SO_3$: 50 $\mu$M). Red channel $\lambda_{em}$ = 630 ± 20 nm ($\lambda_{ex}$ = 561 nm).

upon pretreatment with LPS for 60 min, the fluorescence signal of **NT-$NH_2$-MR**-loaded HepG 2 cells decreased in the red channel. Also, upon incubation with $Na_2SO_3$ for 20 min, the fluorescence intensity in the red channel decreased Figure 5 (c1). Hence, we speculate that **NT-$NH_2$-MR** was potentially suitable for response of exogenous and endogenous $SO_2$ in living cells.

In order to further expand the biological applications of the **NT-$N_3$-SP**, we next examined its capability for visualization of $H_2S$ and $SO_2$ in a mouse model. As shown in Figure 6a1, no fluorescence signals were observed in mice before injection of the **NT-$N_3$-SP** and **NT-$NH_2$-MR**. Then the solutions of **NT-$N_3$-SP** (100 $\mu$M) with or without UV irradiation were separately injected into two groups of tested mice. As shown in Figure 6a2, distinctive fluorescence signal appeared in the mice after injection of **NT-$NH_2$-MR** in group 1. However, another group

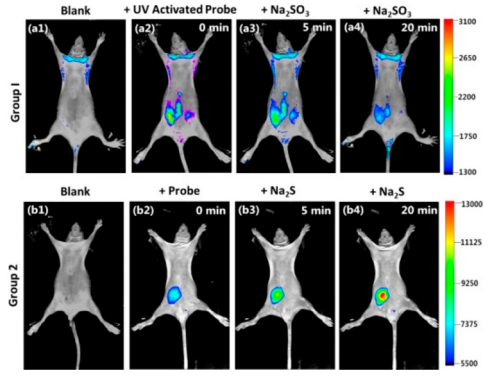


**Figure 6.** Visual imaging of $Na_2SO_3$ and $Na_2S$ in mice model. (a1, b1) Fluorescence imaging of the control group. Fluorescent signals of **NT-$NH_2$-MR** 100 $\mu$M (a2) and **NT-$N_3$-SP** 100 $\mu$M (b2) in living mice. Fluorescent signals of **NT-$NH_2$-MR** 100 $\mu$M (a2) and **NT-$N_3$-SP** 100 $\mu$M (b2) upon injection of $Na_2SO_3$ 200 $\mu$M (a3, a4) and $Na_2S$ 200 $\mu$M (b3, b4) at 5 and 20 min, respectively. Group 1: red channel $\lambda_{em}$ = 600 ± 20 nm ($\lambda_{ex}$ = 530 nm). Group 2: green channel $\lambda_{em}$ = 540 ± 20 nm ($\lambda_{ex}$ = 450 nm).



DOI: 10.1021/acs.orglett.9b01879
Org. Lett. XXXX, XXX, XXX−XXX

of mice per treatment with **NT-$N_3$-SP** exhibited a weak fluorescent signal. After 15 min, we injected $Na_2SO_3$ and $Na_2S$ to the two groups of mice and then anesthetized them for fluorescence imaging. As time went by, the fluorescence intensity in the mice gradually decreased with the injection of $Na_2SO_3$, and remarkable enhancement of fluorescence signals appeared in the other group which was treated with $Na_2S$. Therefore, we envision that **NT-$N_3$-SP** was suitable for screening the increased concentration of $H_2S$ and $SO_2$ in living mice models.

To conclusion, inspired by the light-controlled recognition strategy, for the first time we have successfully engineered a novel fluorescent probe **NT-$N_3$-SP** based on 4-azide-1,8-naphthalic anhydride and spiropyran derivative. The azide group in **NT-$N_3$-SP** could be reduced in the presence of $H_2S$, and the activated spiropyran moiety could serve as a new $SO_2$ recognition site upon UV radiation. Importantly, the "smart" sensor **NT-$N_3$-SP** exhibits high selectivity and sensitivity for $SO_2$ and $H_2S$, and it was also successfully applied to in vivo imaging in living cells and mice. Relying on these merits, we believe that this work provides a powerful tool for better understanding the contributions of $SO_2$ and $H_2S$ in physiological and pathological processes.

## ■ ASSOCIATED CONTENT

### Supporting Information

The Supporting Information is available free of charge on the ACS Publications website at DOI: 10.1021/acs.orglett.9b01879.

Experimental procedures, additional UV−vis and fluorescence spectra, and analytical and spectral data for all compounds (PDF)

## ■ AUTHOR INFORMATION


### Corresponding Author

*E-mail: yincx@sxu.edu.cn.

### ORCID

Caixia Yin: 0000-0001-5548-6333


### Notes

The authors declare no competing financial interest.

## ■ ACKNOWLEDGMENTS

We thank the National Natural Science Foundation of China (Nos. 21775096, 21672131, and 21705102), One hundred people plan of Shanxi Province, Shanxi Province "1331 project" key innovation team construction plan cultivation team (2018-CT-1), Shanxi Province Foundation for Returness (2017-026), the Shanxi Province Science Foundation for Youths (No. 201701D221061), Shanxi Collaborative Innovation Center of High Value-added Utilization of Coal-related Wastes, China Institute for Radiation Production and Scientific Instrument Center of Shanxi University (201512). We also thank Dr. J. J. Wang of Shanxi University for her assistance with confocal laser scanning microscopy imaging.

## ■ REFERENCES

(1) Jiao, X. Y.; Li, Y.; Niu, J. Y.; Xie, X. L.; Wang, X.; Tang, B. *Anal. Chem.* **2018**, *90*, 533−555.
(2) Liu, C. R.; Chen, N. W.; Shi, W.; Peng, B.; Zhao, Y.; Ma, H. M.; Xian, M. *J. Am. Chem. Soc.* **2014**, *136*, 7257−7260.
(3) Fukuto, J. M.; Ignarro, L. J.; Nagy, P.; Wink, D. A.; Kevil, C. G.; Feelisch, M.; Cortese-Krott, M. M.; Bianco, C. L.; Kumagai, Y.; Hobbs, A. J.; Lin, J.; Ida, T.; Akaike, T. *FEBS Lett.* **2018**, *592*, 2140−2152.
(4) Zhao, Y.; Henthorn, H. A.; Pluth, M. D. *J. Am. Chem. Soc.* **2017**, *139*, 16365−16376.
(5) Cerda, M. M.; Zhao, Y.; Pluth, M. D. *J. Am. Chem. Soc.* **2018**, *140*, 12574−12579.
(6) Du, Z. B.; Song, B.; Zhang, W. Z.; Duan, C. C.; Wang, Y. L.; Liu, C. L.; Zhang, R.; Yuan, J. L. *Angew. Chem., Int. Ed.* **2018**, *57*, 3999−4004.
(7) Pardeshi, K. A.; Ravikumar, G.; Chakrapani, H. *Org. Lett.* **2018**, *20*, 4−7.
(8) Li, J. L.; Meng, Z. Q. *Nitric Oxide* **2009**, *20*, 166−174.
(9) Xu, W.; Teoh, C. L.; Peng, J. J.; Su, D. D.; Yuan, L.; Chang, Y. T. *Biomaterials* **2015**, *56*, 1−9.
(10) Chen, S. Y.; Huang, Y. Q.; Liu, Z. W.; Yu, W.; Zhang, H.; Li, K.; Yu, X. Q.; Tang, C. S. *Clin Sci. (Lond).* **2017**, *131*, 2655−2670.
(11) Xiao, J.; Zhu, X. Y.; Kang, B.; Xu, J. B.; Wu, L. H.; Hong, J.; Zhang, Y. F.; Wang, Z. N. *Cell Physiol Biochem* **2015**, *37*, 2444−2453.
(12) Chen, Q. H.; Zhang, L. L.; Chen, S. Y.; Huang, Y. Q.; Li, K.; Yu, X. Q.; Zhang, C. Y.; Tang, C. S.; Du, J. B.; Jin, H. F. *Int. J. Cardiol* **2016**, *225*, 392−401.
(13) Ji, K. X.; Xue, L.; Cheng, J. W.; Bai, Y. *Brain Res. Bull.* **2016**, *121*, 68−74.
(14) Zhang, D.; Wang, X. L.; Tian, X. Y.; Zhang, L. L.; Yang, G. S.; Tao, Y. H.; Liang, C.; Li, K.; Yu, X. Q.; Tang, X. J.; Tang, C. S.; Zhou, J. *Front Immunol* **2018**, *9*, 882−899.
(15) Jiménez, D.; Martínez-Máñez, R.; Sancenón, F.; Ros-Lis, J. V.; Benito, A.; Soto, J. *J. Am. Chem. Soc.* **2003**, *125*, 9000−9001.
(16) Searcy, D. G.; Peterson, M. A. *Anal. Biochem.* **2004**, *324*, 269−275.
(17) Radford-Knoery, J.; Cutter, G. A. *Anal. Chem.* **1993**, *65*, 976−982.
(18) de Macedo, A. N.; Jiwa, M. I. Y.; Macri, J.; Belostotsky, V.; Hill, S.; Britz-McKibbin, P. *Anal. Chem.* **2013**, *85*, 11112−11120.
(19) Jiang, G. W.; Li, M.; Wen, Y. Y.; Zeng, W. L.; Zhao, Q.; Chen, C. L.; Yuan, H.; Liu, C. R.; Liu, C. L. *ACS Sens* **2019**, *4*, 434−440.
(20) Filipovic, M. R.; Zivanovic, J.; Alvarez, B.; Banerjee, R. *Chem. Rev.* **2018**, *118*, 1253−1337.
(21) Ong, J. X.; Lim, C. S. Q.; Le, H. V.; Ang, W. H. *Angew. Chem., Int. Ed.* **2019**, *58*, 164−167.
(22) Zhang, W. J.; Huo, F. J.; Yin, C. X. *J. Mater. Chem. B* **2018**, *6*, 6919−6929.
(23) Jiang, M.; Gu, X.; Lam, J. W. Y.; Zhang, Y.; Kwok, R. T. K.; Wong, K. S.; Tang, B. Z. *Chem. Sci.* **2017**, *8* (8), 5440−5446.
(24) Cheng, P. H.; Zhang, J. J.; Huang, J. G.; Miao, Q. Q.; Xu, C. J.; Pu, K. Y. *Chem. Sci.* **2018**, *9*, 6340−6347.
(25) Gao, M.; Yu, F. B.; Lv, C. J.; Choo, J. B.; Chen, L. X. *Chem. Soc. Rev.* **2017**, *46*, 2237−2271.
(26) Thorson, M. K.; Majtan, T.; Kraus, J. P.; Barrios, A. M. *Angew. Chem., Int. Ed.* **2013**, *52*, 4641−4644.
(27) Brito da Silva, C.; Gil, E. S.; da Silveira Santos, F.; Moras, A. M.; Steffens, L.; Bruno Goncalves, P. F.; Moura, D. J.; Ludtke, D. S.; Rodembusch, F. S. *J. Org. Chem.* **2018**, *83*, 15210−15224.
(28) Irie, M.; Fukaminato, T.; Matsuda, K.; Kobatake, S. *Chem. Rev.* **2014**, *114*, 12174−12277.
(29) Dong, M.; Babalhavaeji, A.; Samanta, S.; Beharry, A. A.; Woolley, G. A. *Acc. Chem. Res.* **2015**, *48*, 2662−2670.
(30) Tian, Z.; Li, A. D. Q. *Acc. Chem. Res.* **2013**, *46*, 269−279.
(31) Zhang, J. J.; Fu, Y. X.; Han, H. H.; Zang, Y.; Li, J.; He, X. P.; Feringa, B. L.; Tian, H. *Nat. Commun.* **2017**, *8* (1), 987−996.
(32) Zhang, W. J.; Liu, T.; Huo, F. J.; Ning, P.; Meng, X. M.; Yin, C. X. *Anal. Chem.* **2017**, *89*, 8079−8083.
(33) Zhang, W. J.; Huo, F. J.; Liu, T.; Yin, C. X. *J. Mater. Chem. B* **2018**, *6*, 8085−8089.



DOI: 10.1021/acs.orglett.9b01879
*Org. Lett.* XXXX, XXX, XXX−XXX